ACS APPLIED MATERIALS & INTERFACES

Research Article

Cite This: ACS Appl. Mater. Interfaces 2018, 10, 21009−21017

www.acsami.org

Stretchable Transparent Electrodes with Solution-Processed Regular Metal Mesh for an Electroluminescent Light-Emitting Film

Cuiping Zhang,[†,‡] Arshad Khan,[†] Jingxuan Cai,[†,‡] Chuwei Liang,[†,‡] Yanjun Liu,[§] Junhong Deng,[∥] Siya Huang,[⊥] Guixin Li,[∥,#] and Wen-Di Li*[,†,‡]

[†]Department of Mechanical Engineering, The University of Hong Kong, Pokfulam, Hong Kong, China

[‡]HKU-Zhejiang Institute of Research and Innovation (HKU-ZIRI), Hangzhou 311300 Zhejiang, China

[§]Department of Electrical and Electronic Engineering, [∥]Department of Materials Science and Engineering, [⊥]SUSTech Academy for Advanced Interdisciplinary Studies, and [#]Shenzhen Institute for Quantum Science and Engineering, Southern University of Science and Technology, Shenzhen 518055 Guangdong, China

Supporting Information

ABSTRACT: We report stretchable metal-mesh transparent electrodes (TEs) with excellent electrical conductivity (<2 Ω/sq) and optical transparency (>80%) under up to 55% strain. The figures of merit on these electrodes, as defined as the ratio between electrical conductivity and optical conductivity, are among the highest reported for stretchable TEs under moderate stretching. Moreover, we demonstrate their application in a stretchable electroluminescent (EL) light-emitting film as top and bottom electrodes. EL lighting devices require low-resistance electrodes to unleash their potential for large-area low-power-consumption applications, in which our highly conductive and transparent stretchable TEs provide an edge on other competitor approaches. Importantly, our stretchable metal-mesh electrodes are fabricated through a vacuum-free solution-processed approach that is scalable for cost-effective mass production. We also investigate the fracture and fatigue mechanisms of stretchable metal-mesh electrodes with various mesh patterns and observe different behaviors under one-time and cyclic stretching conditions. Our solution-processed fabrication method, failure mechanism investigation, and device demonstration for metal-mesh stretchable TEs will facilitate the adoption of this promising high-performance approach in stretchable and wearable electronics applications.

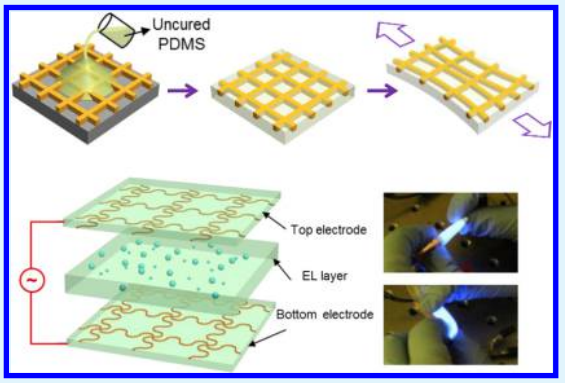

KEYWORDS: *stretchable conductors, metal-mesh electrodes, transparent conductive film, solution-processed fabrication, electroluminescent light emitter*

1. INTRODUCTION

Stretchable and wearable electronics are attracting enormous attention in recent years.[1−3] Many stretchable optical and electronic devices, such as displays,[4,5] solar cells,[6,7] capacitors,[8] antennas,[9] and sensors,[10−12] have been developed to maintain their functions under mechanical deformation and stretching. As a key component in these emerging devices, transparent electrodes (TEs) that can retain high electrical conductivity and optical transmittance under large strain have received intensive research interest. Conductive oxide materials, such as indium tin oxide (ITO), have been the most popular TE choice used for traditional electronic devices given their outstanding transmittance and conductivity performance. However, intrinsic drawbacks of ITO film, such as its brittleness,[13] limited indium resources,[14] and high fabrication expense due to high-temperature or vacuum processing,[15] hinder its future development for flexible and stretchable electronic devices.

In recent years, researchers have investigated a number of alternative TE solutions, such as doped metal oxides,[16,17] metal thin films,[18−20] metal meshes,[21−24] electrospun and spun nanofibers,[25−27] conductive polymers,[28,29] carbon nanotubes,[30,31] graphene flakes,[32,33] and metal nanowires.[34,35] Among these techniques, many have also found applications as stretchable TEs. However, various challenges are still facing their development. Conductive polymer- and carbon nanomaterial-based electrodes suffer from relatively high electrical resistance, which is typically 2 to 3 orders of magnitude higher than that of the ITO film.[28,33] The silver nanowire network is a promising technique that can achieve performance comparable to that of the ITO film[36,37] and shows desirable flexibility and stretchability with elastomeric materials such as polydimethylsiloxane (PDMS)[38] as the substrates. Stretchable silver nanowire TEs have been used in stretchable electroluminescent (EL) devices,[39] stretchable light-emitting diode displays,[4,5,40]

Received: April 24, 2018
Accepted: May 25, 2018
Published: May 25, 2018

DOI: 10.1021/acsami.8b06691
ACS Appl. Mater. Interfaces 2018, 10, 21009−21017

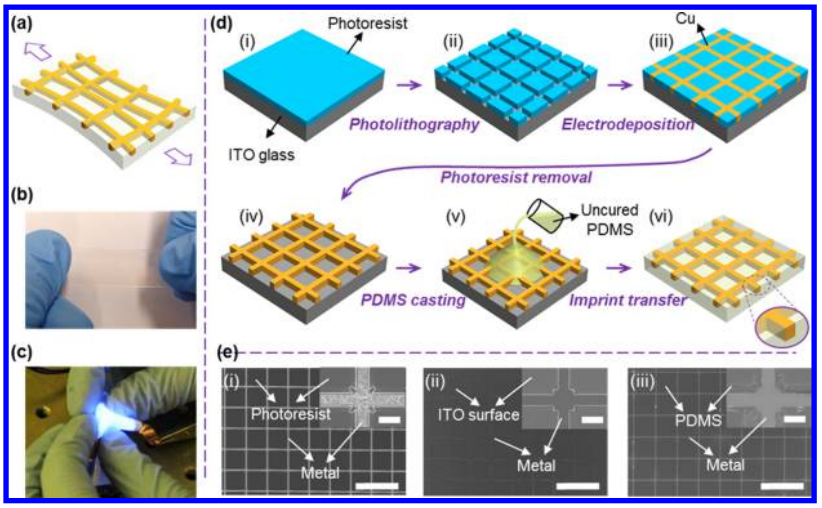

Figure 1. Transparent stretchable metal-mesh electrode and its fabrication. (a) Schematic of a stretched metal-mesh TE. (b) Metal-mesh TE under stretching. (c) Deformed stretchable EL light emitter composed of metal-mesh TEs on both sides. (d) Schematic of the fabrication procedure of the stretchable transparent metal-mesh electrodes, including (i) spin-coating the photoresist on the ITO glass substrate, (ii) creating the microsized trench patterns via photolithography, (iii) electrodeposition of the metal-mesh grid in photoresist trenches, (iv) dissolving the photoresist to leave the metal mesh on the ITO glass surface, (v) casting and curing PDMS, and (vi) separating the final stretchable TE embedded in PDMS from the ITO glass. (e) SEM images of (i) the square metal mesh in photoresist trenches, (ii) the metal mesh on the ITO glass, and (iii) the metal mesh embedded in the PDMS substrate (scale bar: 100 μm for overview images and 6 μm for zoom-in images).

and wearable transparent heaters.[41] However, before they are widely adopted, various problems, such as high contact resistance at nanowire junctions and inhomogeneity and poor reproducibility due to the random arrangement of nanowires, need to be solved. Metal-mesh TEs are another promising alternative technique with electrical and optical performances comparable or superior to that of the ITO film.[42] However, many reported metal-mesh TEs involve expensive and unscalable processing, such as vacuum deposition of metal,[42,43] which needs further development for large-volume, high-throughput, and low-cost production.

Some of the reported electrodes can work at straining ratios much larger than 100%;[40,43−48] however, most of these ultrastretchable electrodes do not have electrical and optical performances comparable to rigid TEs. On the other hand, most targeted applications of stretchable electrode, such as in wearable devices and electronic skins, devices will not be stretched with an extremely large ratio, but typically of no more than 20% for gentle motion[49] and around 55% for large motion.[50] This fact makes it possible to use metal-mesh stretchable electrodes with properly designed regular patterns, which may not sustain ultrahigh stretching but can offer much better electrical and optical performances, particularly if a suitable low-cost fabrication process can be established.

In this work, we adapt a previously reported solution-processed method[51] for fabricating stretchable TEs with regularly patterned metal meshes embedded in an elastomeric substrate (Figure 1a,b) and demonstrate a stretchable electroluminescence light-emitting film. The fabrication process includes three major steps: lithography, electroplating, and elastomer curing and transfer. Stretchable TEs with different metal-mesh patterns, including square, hexagon, zigzag, and serpentine, are fabricated and compared. Their sheet resistance stability is characterized under one-time and cyclic straining conditions. Under the one-time straining of up to 55%, the serpentine electrode, which has an initial sheet resistance below 1 Ω/sq, maintained a low sheet resistance of less than 2 Ω/sq, whereas under the cyclic stretching of 500 repeated cycles at 20% strain, the hexagon metal-mesh electrodes exhibit better stability with the sheet resistance increased from below 1 Ω/sq to approximately 10 Ω/sq, comparing to more than 1000 Ω/sq on zigzag and serpentine meshes only after 200 cycles stretching. Through investigation on the different stretchabilities of stretchable electrodes with various metal-mesh patterns, we discuss the failure mechanisms that cause fracture and fatigue on the microscale metal meshes. Our systematic investigation on the failure mechanisms provides useful guidance on the design and application of metal-mesh electrodes in stretchable electronic devices. Finally, we demonstrate the application of our electrodes in a stretchable EL light-emitting device (Figure 1c). The stretchable light emitter with regular metal-mesh electrodes exhibited desirable foldability and worked without noticeable failure up to a 60% strain.

2. RESULTS AND DISCUSSION

2.1. Cost-Effective and Solution-Processed Lithographic Fabrication of Stretchable Metal-Mesh TEs. We apply a solution-based fabrication strategy for the reported stretchable TEs with embedded metal meshes. The fabrication procedure is adapted from our previous work[51] and illustrated in Figure 1d. First, a photoresist layer is spin-coated on an ITO glass substrate. Then, the designed mesh patterns are created in the photoresist via ultraviolet (UV) photolithography. Metallization is performed through electrodeposition to grow the copper mesh within the photoresist trench. After the photoresist is removed using acetone and the sample is cleaned using isopropyl alcohol, a layer of PDMS prepolymer (Sylgard 184 kit, 10:1 mixed ratio) is casted on the copper mesh and cured after degassing in a vacuum chamber. Finally, the cured PDMS substrate can be peeled off from the ITO substrate with the copper mesh embedded inside because the cured PDMS effectively wraps and confines the copper mesh, thereby leading to enhanced adhesion compared with that at the interface between the copper mesh and ITO. The fabrication process was characterized by scanning electron microscopy (SEM) after

DOI: 10.1021/acsami.8b06691
ACS Appl. Mater. Interfaces 2018, 10, 21009−21017

each major step, and corresponding SEM images are shown in Figure 1e for square-mesh electrodes and in Figures S1 and S2 for other mesh patterns.

The fabrication method presented in this work is a cost-effective solution-based process, and the curing of PDMS can be accomplished at room temperature without using a vacuum environment. Additionally, with this fabrication method, effective control of electrode performance can be achieved by adjusting the pattern designs in the lithography process and altering the metal-mesh dimensions via tuning the electrodeposition parameters. These advantages make our stretchable transparent metal-mesh electrode and its solution-based fabrication very desirable for mass production and device applications.

2.2. Electrical and Optical Characterizations of the Stretchable TEs with Various Metal-Mesh Patterns. Electrical sheet resistance and optical transmittance were characterized for stretchable electrodes of various metal-mesh patterns. Figure 2a shows the morphology of four different photoresist patterns after UV photolithography, namely, square, hexagon, zigzag, and serpentine. In the square pattern, the photoresist trench has a width of 3 μm and a grid pitch of 50 μm. The hexagon and square patterns both have straight connections between lattice junctions, but by eliminating straight lines across the whole electrode, as in the square mesh, we expect the hexagon mesh can deform to allow more stretching. The zigzag and serpentine patterns also have a square lattice, but they feature curved paths with sharp corners and rounded corners, respectively, to replace straight connections between lattice junctions in a square mesh. These curved paths are expected to act as buffers under stretching and improve the stretchability of the metal-mesh electrodes.

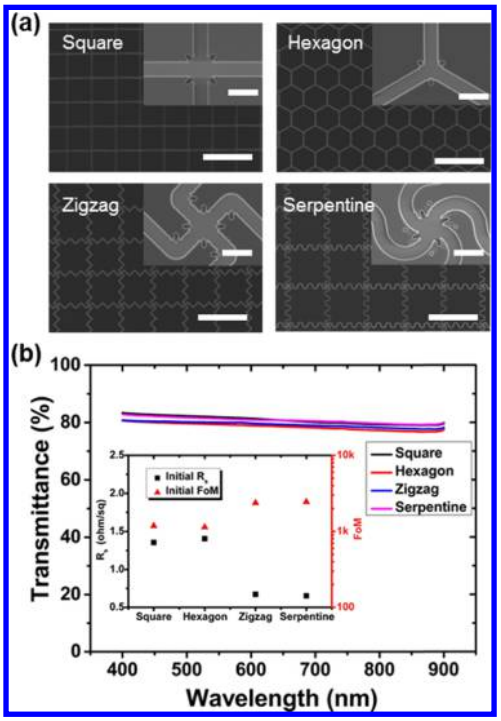

Figure 2. Four different patterns for stretchable metal-mesh TEs. (a) SEM images of the square, hexagon, zigzag, and serpentine patterns exposed in photoresist for subsequent electrodeposition of a metal mesh. (Scale bar: 100 μm for the overview and 6 μm for the zoom-in images.) (b) Transmittance characterization of the stretchable metal-mesh TEs with various mesh patterns. The inset graph shows the initial sheet resistances and the FoMs for square, hexagon, zigzag, and serpentine patterns.

We designed the geometric parameters of the four different patterns so that they have the same line width and filling ratio to avoid influences of these factors on comparison of their electrical behaviors under stretching. As shown in Figure 2b, the normalized transmittance of the four copper-mesh electrodes is all between 80 and 83% at 550 nm wavelength. This indicates that the metal filling ratios on these electrodes are consistent. Characterization shows that the initial sheet resistances of the four electrodes are 1.36 (square), 1.41 (hexagon), 0.67 (zigzag), and 0.65 (serpentine) Ω/sq. The TEs with different meshes initially had nearly the same sheet resistances because of the same mesh thickness and the same filling ratio before the metal meshes were peeled off from the ITO substrates. However, the meshes underwent straining during the PDMS peel-off transfer, and this initial straining induced different changes in the sheet resistances of the four meshes. This will be discussed further in section 2.3. The relatively low resistances of the electrodes are attributed to the good electrical conductivity of copper and the thickness of the copper mesh. Such electrical (~1 Ω/sq) and optical (>80% transmittance) performances are superior to that of the most reported stretchable TEs and are highly desirable in wearable optoelectronic devices. To better evaluate the overall performance of our stretchable TEs, a figure of merit (FoM) commonly used in rigid and flexible TEs, which is the ratio of electrical conductivity to optical conductivity,[37] is calculated by eq 1

$$\mathrm{FoM} = \frac{\sigma_{dc}}{\sigma_{opt}} = \frac{188.5}{R_s\left(\frac{1}{\sqrt{T}} - 1\right)} \quad (1)$$

where R_s and T are the sheet resistance and transmittance of the electrode, respectively. The initial FoMs of various copper-mesh electrodes, together with their initial sheet resistance, are shown in the inset of Figure 2b. Copper-mesh electrodes with four different patterns all show FoMs above 1000, which is well beyond the typical FoM of 350 on a commercial ITO glass.[37] The copper-mesh electrodes also exhibit reasonably good environmental stability. We record that the sheet resistance measured on a square copper-mesh electrode increased from 0.99 to 1.50 Ω/sq after 14-day storage in the ambient environment (Figure S3, Supporting Information), and there is no obvious change of the copper-mesh morphology (Figure S4, Supporting Information).

2.3. Failure Mechanisms of the Metal-Mesh Electrodes under One-Time Straining. Stability of the electrical conductivity under stretching is a critical issue for stretchable electrodes. In device applications, two types of stretchability are involved. One is the stability under a one-time large straining, and the other is the resistance change under cyclic straining. Variation of the sheet resistance on our four types of stretchable TEs under one-time large straining is characterized using a four-probe measurement setup integrated with a manual stretching platform, as shown in Figure 3a. In this setup, an electrode is clamped and fixed on a sliding holder and subjected to a one-time continuous straining with up to 55% total elongation. Silver paste is used on the two sides of the electrode to ensure reliable contact between the electrode and the probes during stretching. To avoid undesirable cracking due to concentrated stress at the clipping locations, we separated the

DOI: 10.1021/acsami.8b06691
ACS Appl. Mater. Interfaces 2018, 10, 21009−21017

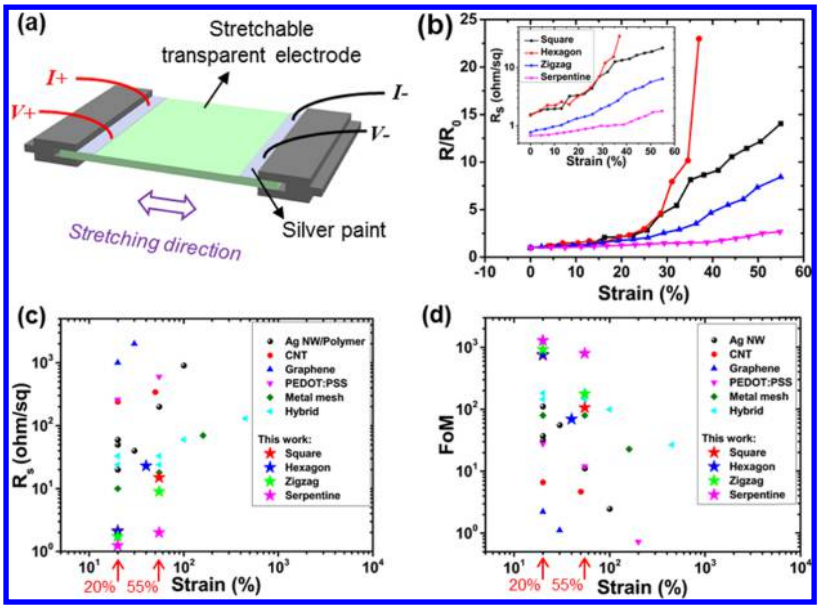

Figure 3. Sheet resistance and FoM characterization of the stretchable TEs under a one-time straining process. (a) Schematic of the experimental setup for stretching the copper-mesh TEs and characterizing their sheet resistance under straining. (b) Variation of sheet resistance vs applied strain ratios for the four types of stretchable TEs. (c) Comparison of sheet resistance under various straining ratios between our electrodes and previously reported stretchable electrodes, namely, AgNW,[40,41,52] CNT,[53] graphene,[33,54] PEDOT:PSS,[29] metal mesh,[43] and hybrid structure.[45,55] (d) Comparison of FoM between our electrodes and previously reported stretchable electrodes under various straining ratios.

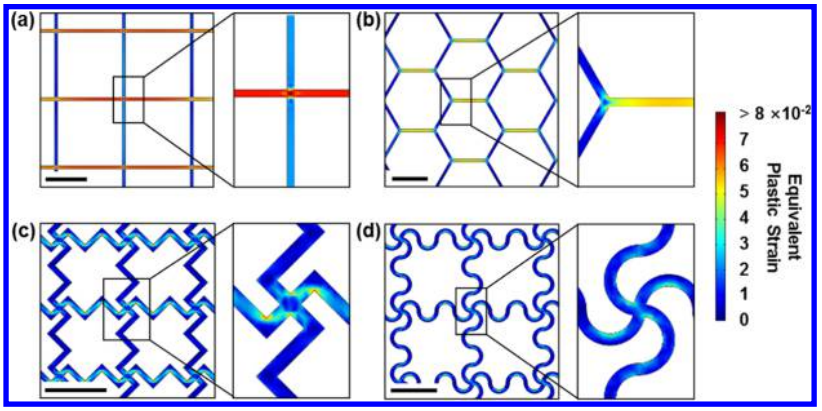

Figure 4. Finite element analysis simulation of the equivalent plastic strain distribution on (a) square, (b) hexagon, (c) zigzag, and (d) serpentine copper meshes embedded in PDMS with 10% total elongation. The color scale shows the equivalent plastic strain (scale bar: 30 μm).

electrical contact on the metal mesh from the clipping location. The electrodes are clipped at a location that is out of the region of the metal mesh under testing.

Figure 3b plots the relative change of the sheet resistance versus the stretching ratio in a one-time straining, with the inset showing the variation of the absolute resistance. As shown in Figure 3b, at 55% strain, the serpentine copper-mesh electrode exhibits the best performance with less than 2 Ω/sq sheet resistance, approximately twice the initial sheet resistance before stretching. The zigzag mesh also shows less resistance increase comparing to that of the square and hexagon meshes. This can be attributed to the curved buffer paths in the serpentine and zigzag meshes, which can deform and absorb the stress induced by the large straining. The copper-mesh electrodes investigated in Figure 3b all have a thickness of 1 μm. We also investigated the thickness dependence of the sheet resistance variation for a serpentine copper-mesh electrode (as shown in Figure S3, Supporting Information), which shows that a generally thinner mesh exhibits more stable sheet resistance under one-time large straining.

In Figure 3c,d, we compare the performance (i.e., the FoM and the sheet resistance) of our copper-mesh stretchable electrodes with previously reported stretchable TEs at two straining ratios of 20 and 55% under one-time straining, respectively. The comparison shows that under moderate stretching conditions, which are most common in wearable electronics applications as discussed earlier, metal-mesh electrodes demonstrated in our work exhibit high FoMs of between 100 and 1000 with low sheet resistances of approximately 10 Ω/sq or less, all among the best reported results.

To understand the failure mechanism that causes resistance increase in the various stretched copper-mesh electrodes, we examine the electrodes under various strains up to 55% using optical microscopy (Figures S6–S10, Supporting Information), where the formation of fractures is clearly observed in the stretched mesh. When the meshes are under a one-time

DOI: 10.1021/acsami.8b06691
ACS Appl. Mater. Interfaces 2018, 10, 21009–21017

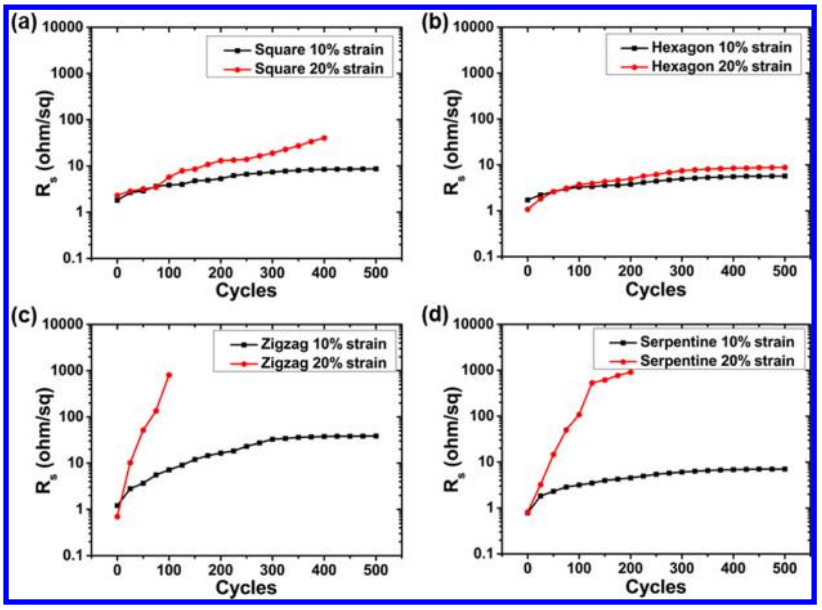

Figure 5. Sheet resistance characterization of the stretchable TEs under a cyclic straining test: (a) square, (b) hexagon, (c) zigzag, and (d) serpentine copper meshes embedded in the PDMS matrix.

continuous straining, the copper lines are initially subjected to elastic deformation and then plastic deformation until fracturing. It has been reported that for copper meshes, plastic strain larger than 10% will lead to observable fractures.[56] Distribution of the local stress and strain varies with the mesh patterns; therefore, the electrodes exhibit different fracture behaviors.

We numerically simulate and compare the distribution of the equivalent plastic strain on the four different meshes under 10% elongation using the finite element analysis method (Figure 4). To simplify the simulation, the copper meshes and PDMS substrates are perfectly bonded without sliding at the bottom and the side interfaces. The left surface of the substrate is fixed, whereas a displacement of 10% total elongation is applied in the horizontal direction on the right surface. The simulated equivalent plastic strain distribution of the square copper mesh is shown in Figure 4a. With the straining along the horizontal direction, the horizontal copper lines experience high stress and fractures occur on these lines (also see Figures S6a and S7, Supporting Information). Once fractures occur, lines are separated at the breaking point. Then, the mesh is partitioned into segments that are connected by reduced mesh lines, and the mesh pattern is largely deformed to absorb the relatively large overall straining. The plastic strain on the hexagon mesh patterns under the same 10% total elongation is similar to that of the square mesh patterns. As shown in Figure S4b, most fractures on the hexagon mesh occur at the junctions or along the horizontal lines, which is consistent with the simulation result presented in Figure 4b.

Zigzag and serpentine meshes exhibit different fracturing behaviors. When stretched, the curved buffer paths can unfurl to absorb the straining (as shown in Figures S6c,d, S9, and S10, Supporting Information). In the simulated plastic strain distributions shown in Figure 4c,d, unlike the square and hexagon meshes, where high and uniform plastic strain is observed along the entire passage between junctions, the plastic strain on the zigzag and serpentine meshes is more localized and mainly concentrated at curved corners and shows a lower value. Therefore, serpentine and zigzag meshes can sustain a larger stretching, as observed in Figure 3b. However, with the localized and concentrated stress at curved corners, when the zigzag and serpentine meshes undergo cyclic stretching, their fatigue behaviors need to be considered, which will result in different performances.

2.4. Stability of the Metal-Mesh Electrodes under Cyclic Straining. We also compared the sheet resistance variation of the four types of copper-mesh electrodes under cyclic straining, as shown in Figure 5. We repeated the stretch-and-release process for up to 500 cycles at 10 and 20% stretching ratios, respectively, and characterized the sheet resistance of the electrodes after every 25 cycles. Under cyclic straining, the zigzag and serpentine copper-mesh electrodes exhibit a faster and more severe resistance increase than square and hexagon electrodes, which is opposite to the observation in the one-time straining test. Specifically, the hexagon copper-mesh electrode exhibits the best sheet resistance stability with the sheet resistance increased to approximately 10 Ω/sq after 500 cycles of repeated stretching to a strain of 20%. The morphology of the metal-mesh electrodes after cyclic loading is also recorded by SEM (Figures S11 and S12, Supporting Information) and shows strong correlation between the visible crack density and the sheet resistance increase.

The different stability behaviors among various mesh patterns and loading types are attributed to the different failure mechanisms of the stretched copper-mesh electrodes. When a fresh copper mesh undergoes a one-time large straining, the fractures of the mesh are due to the immediate material failure, resulting from a sizable plastic strain, whereas in the cyclic straining test, fatigue is the major failure mechanism, leading to the conductivity decrease of the metal-mesh electrodes. The fatigue of a material refers to the progressive failure under repeated loadings when the initial loading is insufficient to cause an immediate failure. The Coffin−Manson relation, $\Delta\varepsilon_p/2 = A(2N)^{-C}$, can be applied to explain and predict the fatigue behavior of our fabricated copper-mesh electrodes. In this relation, $\Delta\varepsilon_p/2$ denotes the plastic strain amplitude in one loading cycle, fatigue life N indicates the number of repeated loading cycles that a material will undergo before it will

DOI: 10.1021/acsami.8b06691
ACS Appl. Mater. Interfaces 2018, 10, 21009−21017

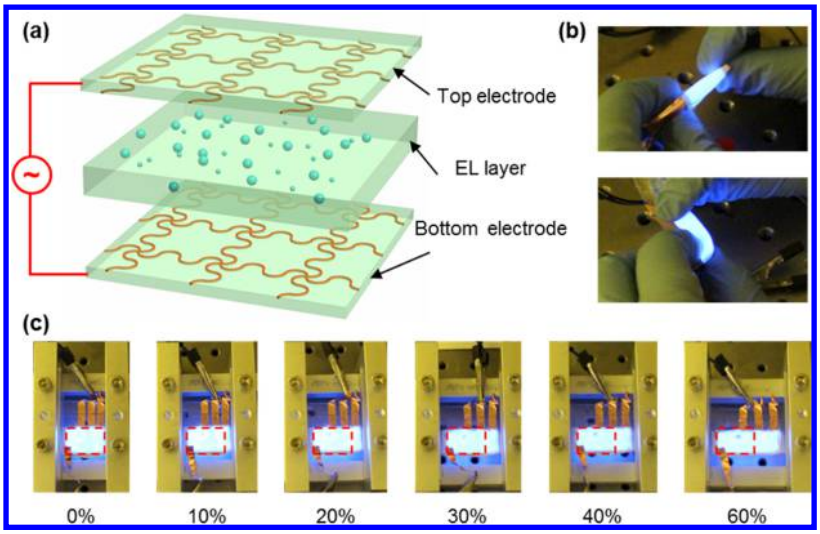

Figure 6. Demonstration of a stretchable EL light emitter using transparent copper-mesh electrodes. (a) Schematic of the structure of the stretchable EL light emitter. (b) EL light emitter folded and wrapped. (c) Light emitter stretched up to 60% strain ratio and showing no obvious degradation.

completely fail, and A and C are positive empirical constants. This model works reasonably well for plastic deformation because of high relative stress. Fatigue life mainly depends on the amplitude of plastic deformation in each loading cycle. Nucleated fractures at positions with a larger plastic strain will occur earlier than those with a smaller plastic strain.

In the square and hexagon copper-mesh electrodes, the fracture in the mesh is more severe during the first few loading cycles. However, after initial fractures are formed in the mesh, the broken lines can slide and create large opening gaps in the subsequent stretching, which helps to mitigate the stress in the surrounding area by deforming the lattice and prolongs fatigue life (Figures S7c and S8d, Supporting Information). Thus, the square and hexagon electrodes exhibit slower resistance increasing under cyclic straining loadings. To further validate this assumption, we simulated a square copper mesh and a hexagon one that undergoes 10% straining (Figure S14, Supporting Information). Both free and periodic boundary conditions are considered in our simulation, and the simulated copper mesh is suspended without the PDMS substrate. We compared the plastic strain distribution of the metal meshes with and without broken lines. As shown in Figure S14, under 10% stretching, once there are fractures formed in the metal mesh, the broken area will undergo larger deformation and the plastic strain of surrounding area will be reduced largely (e.g., from 8 to 1% in the square mesh under both free and periodic boundary conditions). Thus, for square and hexagon meshes, although the plastic strain under initial stretching is large, with fractures formed, the local plastic strain on the mesh will redistribute and be reduced significantly; therefore, the fatigue life is prolonged. This can also be observed through SEM characterization (Figures S11a,b and S12a,b, Supporting Information).

The zigzag and serpentine electrodes are subjected to more localized plastic strain. Although the curved lines unfurl to absorb some applied straining, small fractures may initially nucleate at the corners, where the stress is concentrated, as shown in Figure 4c,d. These fractures may not completely break immediately. In the succeeding repeated cycles, some of the nucleated ruptures will propagate progressively and eventually cause complete fracture of the copper meshes. In the zigzag and serpentine electrodes, copper meshes are more tightly confined inside the PDMS substrate and they cannot easily slide in the PDMS trenches (Figures S11c,d and S12c,d, Supporting Information). Thus, zigzag and serpentine meshes tend to be confined in their original locations, and existing fractures cannot undergo larger deformation and fail to effectively reduce the stress in the surrounding area. For zigzag and serpentine meshes, the fracture formation is more uniform across the whole area and almost in each unit. Consequently, under the cyclic loadings, fractures are continuously formed in the zigzag and serpentine copper-mesh electrodes because of fatigue and result in fast increase in the sheet resistance. Sheet resistance also increases faster when the electrodes are under a repeated strain of 20% than that under 10%, particularly for the zigzag and serpentine electrodes. This is in accordance with the Coffin−Manson relation, which shows that a larger plastic deformation leads to a shorter fatigue life. Additional characterization of the sheet resistance change under cyclic straining loadings for the four mesh patterns is presented in Figure S13, Supporting Information, which shows consistent trend and verifies the reliability of the presented data.

2.5. Stretchable EL Light Emitter Using Metal-Mesh Electrodes. Stretchable EL light emitters were fabricated using the transparent metal-mesh electrodes developed in this work. Figure 6a shows the sandwiched structure of the EL light emitter, where the top and bottom layers are both the copper-mesh electrodes with a serpentine pattern. The light-emitting layer in the middle comprises EL particles dispersed in PDMS. These particles are excited to emit light when an ac voltage is applied to the two electrodes. With the stretchable TEs and the stretchable emissive layer, the light emitter demonstrates good foldability and stretchability, as shown in Figure 6b,c. The EL emitter works properly without noticeable failure under stretching with up to 60% strain ratio. Previous work has demonstrated EL light-emitting devices with desirable stretchability using stretchable electrodes containing silver nanowires[39,57] or ionic conductor.[48,58] These stretchable electrodes often suffer from inhomogeneity, poor reproducibility, and relatively high sheet resistance, which is undesirable for low-power-consumption display and lighting applications. In this work, our lithographically patterned metal mesh offers extremely low sheet resistance under moderate stretching conditions, making it promising to fabricate large-area

DOI: 10.1021/acsami.8b06691
ACS Appl. Mater. Interfaces 2018, 10, 21009−21017

stretchable EL devices by avoiding large voltage drop across the electrodes.

3. CONCLUSIONS

In summary, we design and fabricate stretchable TEs with regular metal-mesh TEs, investigate their failure due to fracture and fatigue, and demonstrate their applications in EL light-emitting film. Our study shows that for most wearable electronic device applications that mainly involve moderate stretching with a stretching ratio of 10−50%, metal-mesh TEs are still one of the best candidate technologies with superior electrical and optical performances. With mesh patterns properly chosen, we demonstrate less than 2 Ω/sq sheet resistance at a one-time 55% stretching on a serpentine copper mesh electrode and approximately 10 Ω/sq sheet resistance on a hexagon copper mesh after 500 times stretching to 20% ratio. Different failure mechanisms under one-time and cyclic stretching conditions are observed and investigated. The FoMs on our electrodes, as defined as the ratio between the electrical conductivity and the optical conductivity, are among the best of the reported stretchable TEs under moderate stretching conditions. We also develop a solution-processed fabrication method, featuring lithography, electrodeposition, and curing and transfer, which is cost-effective and scalable for mass production. The stretchable EL light emitter using our metal-mesh TEs shows desirable foldability and can be stretched up to 60% elongation without noticeable failure.

4. METHODS

4.1. Fabrication of the Stretchable Transparent Metal-Mesh Electrodes. In the photolithography process, a layer of AZ1500 photoresist (~1.8 μm thick) was first spin-coated onto a 3 cm × 3 cm ITO glass at 4000 rpm for 60 s and then baked on the hotplate at 100 °C for 60 s. After the ITO glass was cooled down to room temperature in the air, the photoresist was exposed to 365 nm UV light from a photolithography machine (URE 2000/35, Chinese Academy of Sciences, China) for 9.5 s. The photoresist was immersed and stirred for 40 s in the mixture of AZ351B and deionized (DI) water with a mass ratio of 1:4. Thereafter, the ITO glass was rinsed with DI water and dried in nitrogen gas to obtain the photoresist pattern that corresponded to the designed photomask.

The subsequent metallization process was completed through the electrodeposition of copper onto the ITO glass in the photoresist trenches. A Keithley 2400 sourcemeter was used to apply a constant current source. The ITO glass was dipped in the copper electroplating solution (Plug N′ Plate Flash Copper Solution, Caswell, USA) with the photoresist removed at a corner using acetone. The removed corner has an exposed ITO film and is connected to the current source cathode. A copper wand (Plug N′ Plate Kit, Caswell, USA) was immersed in the electroplating solution and connected to the current source anode. After electroplating, the ITO glass was dipped in acetone for 5 s and subsequently in IPA for 5 s and finally dried carefully in nitrogen, thereby leaving the copper mesh standing on the ITO glass.

The copper mesh was transferred to the elastomeric substrate via polymer curing of PDMS. A PDMS prepolymer mixture (Sylgard 184 kit, PDMS/curing agent mixed with a mass ratio of 10:1) was coated onto the ITO glass to form a layer of 1 mm thick. Then, the PDMS mixture was degassed in a well-sealed vacuum oven for 1 h and then heated at 120 °C for 4 h to cure the PDMS mixture. Curing can be achieved without a vacuum oven or heating by leaving the sample at room temperature for 48 h. Finally, the PDMS elastomer with fully embedded copper mesh can be directly peeled off from the ITO glass.

4.2. Fabrication of the Stretchable EL Emitter. The emissive layer of the stretchable emitter comprises EL particles dispersed in the PDMS elastomer. ZnS/Cu EL particles (Shanghai KPT Company) were mixed with the PDMS prepolymer mixture with a mass ratio of 2:1. Then, the emissive mixture was spin-coated onto the ITO glass with the copper mesh on it at 1000 rpm for 60 s. Then, a fabricated stretchable copper-mesh TE was placed on the ITO glass, with the uncured emissive layer in contact with the embedded copper mesh. After the sample was effectively degassed and completely cured, the ITO glass was separated from the sample. Finally, the sample was encapsulated with another layer of spin-coated and cured PDMS elastomer. The two metal-mesh electrodes were connected using a conductive copper tape to an external ac voltage supply (DG2-3-T, Shanghai KPT Company).

■ ASSOCIATED CONTENT

Supporting Information

The Supporting Information is available free of charge on the ACS Publications website at DOI: 10.1021/acsami.8b06691.

SEM images of electrodeposited Cu mesh on the ITO glass before and after the removal of the photoresist pattern, change of the sheet resistance and the morphology of a square copper mesh stored in the ambient environment, sheet resistance change with the strain on metal meshes of different thickness values, optical microscopy images of the stretched metal-mesh electrodes, SEM images and resistance change of the metal meshes after cyclic straining loadings, and simulation of plastic strain distribution of free-standing metal mesh under 10% stretching with and without predefined cracks (PDF)

■ AUTHOR INFORMATION

Corresponding Author

*E-mail: liwd@hku.hk.

ORCID

Jingxuan Cai: 0000-0003-3554-1379

Guixin Li: 0000-0001-9689-8705

Wen-Di Li: 0000-0002-7005-2784

Notes

The authors declare no competing financial interest.

■ ACKNOWLEDGMENTS

This work was partially supported by the Research Grants Council of Hong Kong (grant nos. 27205515 and 17246116), the National Natural Science Foundation of China (grant no. 61306123), the Department of Science and Technology of Zhejiang Province (grant no. 2017C01058), the Natural Science Foundation of Guangdong Province (grant no. 2017A030313034), the Science and Technology Department of Guangdong Province (grant no. 2017B090918001), and the Science and Technology Innovation Commission of Shenzhen Municipality (grant nos. JCYJ20170412153113701 and JCYJ20170817111349280).

■ REFERENCES

(1) Liu, Y.; Pharr, M.; Salvatore, G. A. Lab-on-Skin: A Review of Flexible and Stretchable Electronics for Wearable Health Monitoring. *ACS Nano* **2017**, *11*, 9614−9635.

(2) Chen, D.; Liang, J.; Pei, Q. Flexible and Stretchable Electrodes for Next Generation Polymer Electronics: A Review. *Sci. China: Chem.* **2016**, *59*, 659−671.

(3) Sannicolo, T.; Lagrange, M.; Cabos, A.; Celle, C.; Simonato, J.-P.; Bellet, D. Metallic Nanowire-Based Transparent Electrodes for Next Generation Flexible Devices: A Review. *Small* **2016**, *12*, 6052−6075.

(4) Choi, M.; Jang, B.; Lee, W.; Lee, S.; Kim, T. W.; Lee, H.-J.; Kim, J.-H.; Ahn, J.-H. Stretchable Active Matrix Inorganic Light-Emitting Diode Display Enabled by Overlay-Aligned Roll-Transfer Printing. *Adv. Funct. Mater.* **2017**, *27*, 1606005.
(5) White, M. S.; Kaltenbrunner, M.; Glowacki, E. D.; Gutnichenko, K.; Kettlgruber, G.; Graz, I.; Aazou, S.; Ulbricht, C.; Egbe, D. A. M.; Miron, M. C.; Major, Z.; Scharber, M. C.; Sekitani, T.; Someya, T.; Bauer, S.; Sariciftci, N. S. Ultrathin, Highly Flexible and Stretchable Pleds. *Nat. Photonics* **2013**, *7*, 811−816.
(6) Lipomi, D. J.; Bao, Z. Stretchable, Elastic Materials and Devices for Solar Energy Conversion. *Energy Environ. Sci.* **2011**, *4*, 3314−3328.
(7) Nam, J.; Seo, B.; Lee, Y.; Kim, D.-H.; Jo, S. Cross-Buckled Structures for Stretchable and Compressible Thin Film Silicon Solar Cells. *Sci. Rep.* **2017**, *7*, 7575.
(8) Chen, T.; Xue, Y.; Roy, A. K.; Dai, L. Transparent and Stretchable High-Performance Supercapacitors Based on Wrinkled Graphene Electrodes. *ACS Nano* **2014**, *8*, 1039−1046.
(9) Jang, T.; Zhang, C.; Youn, H.; Zhou, J.; Guo, L. J. Semitransparent and Flexible Mechanically Reconfigurable Electrically Small Antennas Based on Tortuous Metallic Micromesh. *IEEE Trans. Antennas Propag.* **2017**, *65*, 150−158.
(10) Choi, D. Y.; Kim, M. H.; Oh, Y. S.; Jung, S.-H.; Jung, J. H.; Sung, H. J.; Lee, H. W.; Lee, H. M. Highly Stretchable, Hysteresis-Free Ionic Liquid-Based Strain Sensor for Precise Human Motion Monitoring. *ACS Appl. Mater. Interfaces* **2017**, *9*, 1770−1780.
(11) Choi, T. Y.; Hwang, B.-U.; Kim, B.-Y.; Trung, T. Q.; Nam, Y. H.; Kim, D.-N.; Eom, K.; Lee, N.-E. Stretchable, Transparent, and Stretch-Unresponsive Capacitive Touch Sensor Array with Selectively Patterned Silver Nanowires/Reduced Graphene Oxide Electrodes. *ACS Appl. Mater. Interfaces* **2017**, *9*, 18022−18030.
(12) Zhao, S.; Li, J.; Cao, D.; Zhang, G.; Li, J.; Li, K.; Yang, Y.; Wang, W.; Jin, Y.; Sun, R.; Wong, C.-P. Recent Advancements in Flexible and Stretchable Electrodes for Electromechanical Sensors: Strategies, Materials, and Features. *ACS Appl. Mater. Interfaces* **2017**, *9*, 12147−12164.
(13) Cairns, D. R.; Witte, R. P.; Sparacin, D. K.; Sachsman, S. M.; Paine, D. C.; Crawford, G. P.; Newton, R. R. Strain-Dependent Electrical Resistance of Tin-Doped Indium Oxide on Polymer Substrates. *Appl. Phys. Lett.* **2000**, *76*, 1425−1427.
(14) Kumar, A.; Zhou, C. The Race to Replace Tin-Doped Indium Oxide: Which Material Will Win? *ACS Nano* **2010**, *4*, 11−14.
(15) Ye, S.; Rathmell, A. R.; Chen, Z.; Stewart, I. E.; Wiley, B. J. Metal Nanowire Networks: The Next Generation of Transparent Conductors. *Adv. Mater.* **2014**, *26*, 6670−6687.
(16) Hagendorfer, H.; Lienau, K.; Nishiwaki, S.; Fella, C. M.; Kranz, L.; Uhl, A. R.; Jaeger, D.; Luo, L.; Gretener, C.; Buecheler, S.; Romanyuk, Y. E.; Tiwari, A. N. Highly Transparent and Conductive Zno: Al Thin Films from a Low Temperature Aqueous Solution Approach. *Adv. Mater.* **2014**, *26*, 632−636.
(17) Kevin, M.; Lee, G. H.; Ho, G. W. Non-Planar Geometries of Solution Processable Transparent Conducting Oxide: From Film Characterization to Architectured Electrodes. *Energy Environ. Sci.* **2012**, *5*, 7196−7202.
(18) O'Connor, B.; Haughn, C.; An, K.-H.; Pipe, K. P.; Shtein, M. Transparent and Conductive Electrodes Based on Unpatterned, Thin Metal Films. *Appl. Phys. Lett.* **2008**, *93*, 223304.
(19) Ghosh, D. S.; Martinez, L.; Giurgola, S.; Vergani, P.; Pruneri, V. Widely Transparent Electrodes Based on Ultrathin Metals. *Opt. Lett.* **2009**, *34*, 325−327.
(20) Zhang, C.; Zhao, D.; Gu, D.; Kim, H.; Ling, T.; Wu, Y.-K. R.; Guo, L. J. An Ultrathin, Smooth, and Low-Loss Al-Doped Ag Film and Its Application as a Transparent Electrode in Organic Photovoltaics. *Adv. Mater.* **2014**, *26*, 5696−5701.
(21) Sciacca, B.; van de Groep, J.; Polman, A.; Garnett, E. C. Solution-Grown Silver Nanowire Ordered Arrays as Transparent Electrodes. *Adv. Mater.* **2016**, *28*, 905−909.
(22) Lordan, D.; Burke, M.; Manning, M.; Martin, A.; Amann, A.; O'Connell, D.; Murphy, R.; Lyons, C.; Quinn, A. J. Asymmetric Pentagonal Metal Meshes for Flexible Transparent Electrodes and Heaters. *ACS Appl. Mater. Interfaces* **2017**, *9*, 4932−4940.
(23) Han, B.; Pei, K.; Huang, Y.; Zhang, X.; Rong, Q.; Lin, Q.; Guo, Y.; Sun, T.; Guo, C.; Carnahan, D.; Giersig, M.; Wang, Y.; Gao, J.; Ren, Z.; Kempa, K. Uniform Self-Forming Metallic Network as a High-Performance Transparent Conductive Electrode. *Adv. Mater.* **2014**, *26*, 873−877.
(24) Xian, Z.; Han, B.; Li, S.; Yang, C.; Wu, S.; Lu, X.; Gao, X.; Zeng, M.; Wang, Q.; Bai, P.; Naughton, M. J.; Zhou, G.; Liu, J.-M.; Kempa, K.; Gao, J. A Practical Ito Replacement Strategy: Sputtering-Free Processing of a Metallic Nanonetwork. *Adv. Mater. Technol.* **2017**, *2*, 1700061.
(25) Huh, J. W.; Lee, D. K.; Jeon, H.-J.; Ahn, C. W. New Approach for Fabricating Hybrid-Structured Metal Mesh Films for Flexible Transparent Electrodes by the Combination of Electrospinning and Metal Deposition. *Nanotechnology* **2016**, *27*, 475302.
(26) Wu, H.; Hu, L.; Rowell, M. W.; Kong, D.; Cha, J. J.; McDonough, J. R.; Zhu, J.; Yang, Y.; McGehee, M. D.; Cui, Y. Electrospun Metal Nanofiber Webs as High-Performance Transparent Electrode. *Nano Lett.* **2010**, *10*, 4242−4248.
(27) Bai, X.; Liao, S.; Huang, Y.; Song, J.; Liu, Z.; Fang, M.; Xu, C.; Cui, Y.; Wu, H. Continuous Draw Spinning of Extra-Long Silver Submicron Fibers with Micrometer Patterning Capability. *Nano Lett.* **2017**, *17*, 1883−1891.
(28) Zhang, X.; Wu, J.; Wang, J.; Zhang, J.; Yang, Q.; Fu, Y.; Xie, Z. Highly Conductive PEDOT: PSS Transparent Electrode Prepared by a Post-Spin-Rinsing Method for Efficient Ito-Free Polymer Solar Cells. *Sol. Energy Mater. Sol. Cells* **2016**, *144*, 143−149.
(29) Lipomi, D. J.; Lee, J. A.; Vosgueritchian, M.; Tee, B. C.-K.; Bolander, J. A.; Bao, Z. Electronic Properties of Transparent Conductive Films of PEDOT: PSS on Stretchable Substrates. *Chem. Mater.* **2012**, *24*, 373−382.
(30) Mirri, F.; Ma, A. W. K.; Hsu, T. T.; Behabtu, N.; Eichmann, S. L.; Young, C. C.; Tsentalovich, D. E.; Pasquali, M. High-Performance Carbon Nanotube Transparent Conductive Films by Scalable Dip Coating. *ACS Nano* **2012**, *6*, 9737−9744.
(31) Yu, L.; Shearer, C.; Shapter, J. Recent Development of Carbon Nanotube Transparent Conductive Films. *Chem. Rev.* **2016**, *116*, 13413−13453.
(32) Eda, G.; Fanchini, G.; Chhowalla, M. Large-Area Ultrathin Films of Reduced Graphene Oxide as a Transparent and Flexible Electronic Material. *Nat. Nanotechnol.* **2008**, *3*, 270−274.
(33) Liu, J.; Yi, Y.; Zhou, Y.; Cai, H. Highly Stretchable and Flexible Graphene/ITO Hybrid Transparent Electrode. *Nanoscale Res. Lett.* **2016**, *11*, 108.
(34) Wu, S.; Li, L.; Xue, H.; Liu, K.; Fan, Q.; Bai, G.; Wang, J. Size Controllable, Transparent, and Flexible 2D Silver Meshes Using Recrystallized Ice Crystals as Templates. *ACS Nano* **2017**, *11*, 9898−9905.
(35) Tiwari, N.; Ankit, A.; Rajput, M.; Kulkarni, M. R.; John, R. A.; Mathews, N. Healable and Flexible Transparent Heaters. *Nanoscale* **2017**, *9*, 14990−14997.
(36) Lee, J.-Y.; Connor, S. T.; Cui, Y.; Peumans, P. Solution-Processed Metal Nanowire Mesh Transparent Electrodes. *Nano Lett.* **2008**, *8*, 689−692.
(37) De, S.; Higgins, T. M.; Lyons, P. E.; Doherty, E. M.; Nirmalraj, P. N.; Blau, W. J.; Boland, J. J.; Coleman, J. N. Silver Nanowire Networks as Flexible, Transparent, Conducting Films: Extremely High DC to Optical Conductivity Ratios. *ACS Nano* **2009**, *3*, 1767−1774.
(38) Xu, F.; Zhu, Y. Highly Conductive and Stretchable Silver Nanowire Conductors. *Adv. Mater.* **2012**, *24*, 5117−5122.
(39) Wang, J.; Yan, C.; Chee, K. J.; Lee, P. S. Highly Stretchable and Self-Deformable Alternating Current Electroluminescent Devices. *Adv. Mater.* **2015**, *27*, 2876−2882.
(40) Liang, J.; Li, L.; Niu, X.; Yu, Z.; Pei, Q. Elastomeric Polymer Light-Emitting Devices and Displays. *Nat. Photonics* **2013**, *7*, 817−824.
(41) Hong, S.; Lee, H.; Lee, J.; Kwon, J.; Han, S.; Suh, Y. D.; Cho, H.; Shin, J.; Yeo, J.; Ko, S. H. Highly Stretchable and Transparent

DOI: 10.1021/acsami.8b06691
ACS Appl. Mater. Interfaces 2018, 10, 21009−21017

Metal Nanowire Heater for Wearable Electronics Applications. *Adv. Mater.* **2015**, *27*, 4744−4751.
(42) Kang, M.-G.; Guo, L. J. Nanoimprinted Semitransparent Metal Electrodes and Their Application in Organic Light-Emitting Diodes. *Adv. Mater.* **2007**, *19*, 1391−1396.
(43) Guo, C. F.; Sun, T.; Liu, Q.; Suo, Z.; Ren, Z. Highly Stretchable and Transparent Nanomesh Electrodes Made by Grain Boundary Lithography. *Nat. Commun.* **2014**, *5*, 3121.
(44) Hu, L.; Yuan, W.; Brochu, P.; Gruner, G.; Pei, Q. Highly Stretchable, Conductive, and Transparent Nanotube Thin Films. *Appl. Phys. Lett.* **2009**, *94*, 161108.
(45) Lee, P.; Ham, J.; Lee, J.; Hong, S.; Han, S.; Suh, Y. D.; Lee, S. E.; Yeo, J.; Lee, S. S.; Lee, D.; Ko, S. H. Highly Stretchable or Transparent Conductor Fabrication by a Hierarchical Multiscale Hybrid Nanocomposite. *Adv. Funct. Mater.* **2014**, *24*, 5671−5678.
(46) Cai, L.; Song, L.; Luan, P.; Zhang, Q.; Zhang, N.; Gao, Q.; Zhao, D.; Zhang, X.; Tu, M.; Yang, F.; Zhou, W.; Fan, Q.; Luo, J.; Zhou, W.; Ajayan, P. M.; Xie, S. Super-Stretchable, Transparent Carbon Nanotube-Based Capacitive Strain Sensors for Human Motion Detection. *Sci. Rep.* **2013**, *3*, 3048.
(47) Lee, P.; Lee, J.; Lee, H.; Yeo, J.; Hong, S.; Nam, K. H.; Lee, D.; Lee, S. S.; Ko, S. H. Highly Stretchable and Highly Conductive Metal Electrode by Very Long Metal Nanowire Percolation Network. *Adv. Mater.* **2012**, *24*, 3326−3332.
(48) Wang, J.; Yan, C.; Cai, G.; Cui, M.; Lee-Sie Eh, A.; Lee, P. S. Extremely Stretchable Electroluminescent Devices with Ionic Conductors. *Adv. Mater.* **2016**, *28*, 4490−4496.
(49) Kim, J.; Lee, M.; Shim, H. J.; Ghaffari, R.; Cho, H. R.; Son, D.; Jung, Y. H.; Soh, M.; Choi, C.; Jung, S.; Chu, K.; Jeon, D.; Lee, S.-T.; Kim, J. H.; Choi, S. H.; Hyeon, T.; Kim, D.-H. Stretchable Silicon Nanoribbon Electronics for Skin Prosthesis. *Nat. Commun.* **2014**, *5*, 5747.
(50) Zeng, W.; Shu, L.; Li, Q.; Chen, S.; Wang, F.; Tao, X.-M. Fiber-Based Wearable Electronics: A Review of Materials, Fabrication, Devices, and Applications. *Adv. Mater.* **2014**, *26*, 5310−5336.
(51) Khan, A.; Lee, S.; Jang, T.; Xiong, Z.; Zhang, C.; Tang, J.; Guo, L. J.; Li, W.-D. High-Performance Flexible Transparent Electrode with an Embedded Metal Mesh Fabricated by Cost-Effective Solution Process. *Small* **2016**, *12*, 3021−3030.
(52) Akter, T.; Kim, W. S. Reversibly Stretchable Transparent Conductive Coatings of Spray-Deposited Silver Nanowires. *ACS Appl. Mater. Interfaces* **2012**, *4*, 1855−1859.
(53) Yu, Z.; Niu, X.; Liu, Z.; Pei, Q. Intrinsically Stretchable Polymer Light-Emitting Devices Using Carbon Nanotube-Polymer Composite Electrodes. *Adv. Mater.* **2011**, *23*, 3989−3994.
(54) Kim, K. S.; Zhao, Y.; Jang, H.; Lee, S. Y.; Kim, J. M.; Kim, K. S.; Ahn, J.-H.; Kim, P.; Choi, J.-Y.; Hong, B. H. Large-Scale Pattern Growth of Graphene Films for Stretchable Transparent Electrodes. *Nature* **2009**, *457*, 706−710.
(55) Lee, M.-S.; Lee, K.; Kim, S.-Y.; Lee, H.; Park, J.; Choi, K.-H.; Kim, H.-K.; Kim, D.-G.; Lee, D.-Y.; Nam, S.; Park, J.-U. High-Performance, Transparent, and Stretchable Electrodes Using Graphene-Metal Nanowire Hybrid Structures. *Nano Lett.* **2013**, *13*, 2814−2821.
(56) Gonzalez, M.; Axisa, F.; Bulcke, M. V.; Brosteaux, D.; Vandevelde, B.; Vanfleteren, J. Design of Metal Interconnects for Stretchable Electronic Circuits. *Microelectron. Reliab.* **2008**, *48*, 825−832.
(57) Stauffer, F.; Tybrandt, K. Bright Stretchable Alternating Current Electroluminescent Displays Based on High Permittivity Composites. *Adv. Mater.* **2016**, *28*, 7200−7203.
(58) Yang, C. H.; Chen, B.; Zhou, J.; Chen, Y. M.; Suo, Z. Electroluminescence of Giant Stretchability. *Adv. Mater.* **2016**, *28*, 4480−4484.

DOI: 10.1021/acsami.8b06691
ACS Appl. Mater. Interfaces 2018, 10, 21009−21017